

Diaphragm Ankle Actuation for Efficient Series Elastic Legged Robot Hopping

Marco Bolognari^{1,2}, An Mo³, Marco Fontana² and Alexander Badri-Spröwitz³

Abstract—The observation of the anatomy of agile animals and their locomotion capabilities emphasizes the importance of fast and lightweight legs and confirms the intrinsic compliance integrated into muscle-tendon units as a major ingredient for energy efficient and robust locomotion. This quality is especially relevant for distal leg segments which are subject to aggressive dynamics. Legged robots are accordingly designed to improve dynamic performance by lightweight mechanisms combined with series elastic actuation systems. However, so far no designs are available that feature all characteristics of a perfect distal legged locomotion actuator such as a lightweight and low-inertia structure, with high mechanical efficiency, no stick and sliding friction, and low mechanical complexity. With this goal in mind, we propose a novel robotic leg which integrates all above features. Specifically, we develop, implement, and characterize a bioinspired robot leg that features a lightweight Series ELastic Diaphragm distal Actuator (SELDa) for active control of foot motion. We conducted experiments to compare two leg configurations, with and without foot actuation, to demonstrate the effectiveness of the proposed solution in agile forward hopping controlled by a central pattern generator. We studied how tuning SELDA’s activation timing can adjust the robot’s hopping height by 11% and its forward velocity by 14%, even with comparatively low power injection to the distal joint.

I. INTRODUCTION

Lightweight actuation of distal joints is proven effective by animals and humans, which can run, jump, and hop with agility, robustness and efficiency based on muscle-tendon structures embedded in multi-segment legs. Animals feature low mass and moment of inertia at distal locations, with heavy actuators (muscles) mounted proximally [1], [2], [3]. These muscle-tendon units can be presented as series elastic actuators [2], [4]. The exact functionality of the leg segment architecture, networks of muscle-tendon units, and their mechanical and control coupling are not yet understood and are the focus of ongoing research [5], [6], [7], [8]. In human walking, much research focuses on ankle kinematics and dynamics, the coupling of proximal and distal leg joints through elastic structures and control [9], [10], and the resulting impact on locomotion efficiency, agility, and robustness [11], [12], [13]. In this context, catapult-like power

This work was supported by Department of Excellence grant of Scuola Superiore Sant’Anna, the International Max Planck Research School for Intelligent Systems, the China Scholarship Council, and the Max Planck Society. Gefördert durch die Deutsche Forschungsgemeinschaft (DFG)-449912641.

¹ Department of Industrial Engineering, University of Trento, 38123 Trento, Italy. [marco.bolognari]@unitn.it

² Institute of Mechanical Intelligence, Scuola Superiore Sant’Anna, 56127 Pisa, Italy. [marco.fontana]@santannapisa.it

³ Dynamic Locomotion Group, Max Planck Institute for Intelligent Systems, 70569 Stuttgart, Germany. [mo] [sprowitz]@is.mpg.de

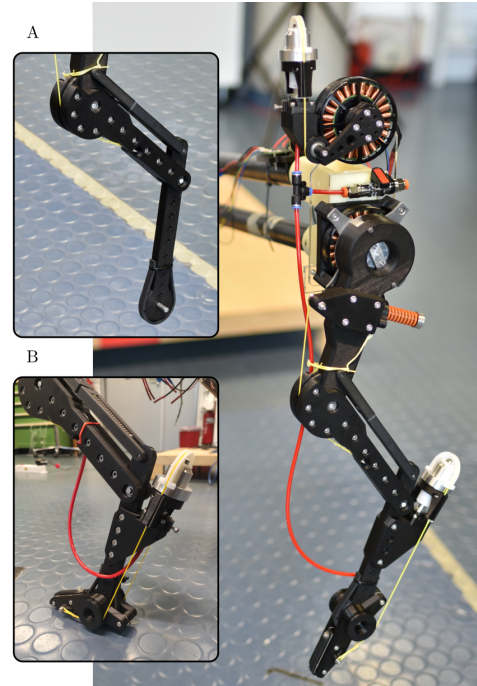


Fig. 1. Experimental prototype of the bio-inspired leg. Detail figures on the left show the two configurations compared in this work. *Configuration-A*: traditional bio-inspired layout. *Configuration-B*: novel configuration with ‘foot’ segment remotely actuated by a compliant pneumatic transmission.

output rooted in lower-leg muscle-tendon structures has been observed that exceeds the muscle’s power output, by charging and discharging lower-leg series elasticities favourably [14], [15], [8]. These examples from biomechanics emphasize the potential to reduce energetic losses, simplify control and mechanics, and increase robustness and agility by leveraging on distally acting series elastic actuators in legged machines.

In robotic legs, the actuation of distal joints is often avoided because combinations of motors and gearboxes, perhaps combined with mechanical series elasticity [16], [17], come with high mass, moment of inertia, and mechanical complexity. Heavy actuators placed distally are energetically costly to be accelerated and decelerated through leg swing. For this reason, several power transmissions have been proposed for the remote actuation of distal joint with proximally located motors, Tab. I. Such transmissions can be achieved with cable (tendon), chain, and belt systems [7], [18], [19], but the design and control complexity of these systems increases notably when transferring the actuation over multiple joints. Simpler systems are possible when remote actuation bypasses joints by transmitting power di-

rectly into the target location. For this reason, Bowden-cable power transmissions have been explored [20], however, high friction between the inner cable and the outer sheath leads to control difficulties and power losses that are prohibitive for mobile application [20]. Alternatively, hydraulic [21], [22] or pneumatic [23] cylinders and pneumatic artificial muscles (PAMs) [24] can be employed for distal actuation. Generally, fluidic actuation is less energy efficient and is associated with complex and bulky parts such as heavy pumps, manifolds, and accumulators that can be only integrated into large-scale robotic systems.

Rolling diaphragm transmissions [25], [26] are novel passive devices that allow the proximal placement of electrical motors with low-friction actuation. Rolling diaphragm actuation of distal joints combines the efficient power transmission of cable/tendon mechanisms with the flexibility of Bowden cables. Both hydraulic and pneumatic configurations are feasible [25]; high bandwidth and stiffness are achieved in the former case, and compliance and energy-storage capabilities are offered in the latter. Promising characteristics of high power, efficiency, mechanical transparency, excellent backdrivability, and simplified control and mechanical design [27] lead to robotic applications such as MRI-compatible backdrivable arms [28], fluid dampers [29], bio-inspired robots [26], and interactive robots [30].

TABLE I
MULTI LEG-JOINT ACTUATION SYSTEMS FOR LEGGED ROBOTS.

Technology	Weight	Design complexity	Force transparency
Coupled multi-joint motion			
Linkage [31]	fair	fair*, poor [†]	good
Tendon [7], chain [18], belt [19]	good	fair*, poor [†]	good
Decoupled multi-joint motion			
PAM [24]	good	poor	poor
Bowden cable [20]	good	good	poor
Hydraulic piston [22]	fair	fair	poor
Rolling diaphragm transmission	good	good	good

*in planar transmission, [†]in 3D transmission or over multiple joints.

In this work, we developed a first proof of concept of Series **E**lastic **D**iaphragm for distal Actuation (SELD) that integrates the positive attributes of diaphragm transmission with a purposely tuned stiffness that provides the sought series elastic actuation (SEA) behaviour. With SELDA, we aim to develop hardware for agile legged hopping that is easy to control, is uncoupled from neighboring joint's movements and loads, is easy and flexible to mount, features a remote motor placement and a distal power output, is distally lightweight, inherently compliant, and mechanically efficient. To test our design, we built a lightweight bio-inspired leg with a remotely actuated foot segment. The foot's actuator is placed in the robot's torso and its torque is reflected at the ankle joint using a pneumatic rolling-diaphragm transmission with intrinsic compliance characteristics.

In the following sections, we present the mechanical design and controller details of SELDA, our series elastic diaphragm for ankle actuation. We present experiment-based characterizations of the pneumatic transmission and actuation, and a comparison of hopping performances between

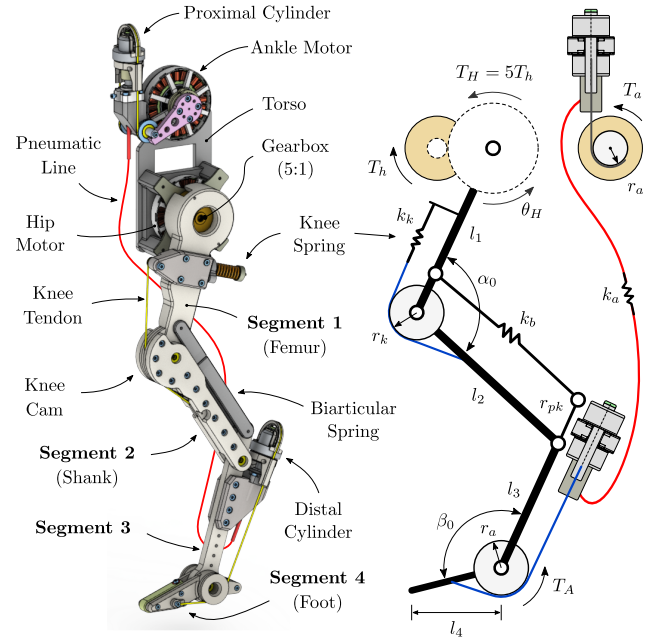


Fig. 2. Drawing of the proposed robotic leg equipped with the SELDA-actuated foot. *Left:* computer-aided design (CAD) picture. *Right:* schematic drawing.

two leg configurations (Fig. 1): configuration-A is a leg without a foot segment, inspired by our previous work [32], while configuration-B is a leg with a foot segment, actuated by SELDA. We compare both configurations by recording locomotion data of both robot legs when hopping forward. Configuration-B is tested a) in passive mode, i.e. without foot-motor actuation, to assess its compliance features, and b) in active mode, i.e., the ankle motor is actively controlled, to explore the effects of foot-actuation timing during the step cycle.

II. ROBOT DESIGN

Lightweight, under-actuated, compliant design of bio-inspired robotic legs proved effective for achieving agile locomotion with low control complexity [23], [33], [32]. However, previous leg designs have not explored the opportunity of introducing ankle actuation which is typically avoided due to the difficulty of independently actuating distal joints with low additional mechanical complexity and inertia.

In this work, we present a bio-inspired leg that is inspired by the design presented in [32] and further enriched by introducing a remotely-actuated, active ankle joint.

A. Leg architecture

Detailed schematics of the proposed robot leg are shown in Fig. 2. The robot features four-segment planar kinematics that mimics the compliant behavior of mammalian quadruped legs. In our design, two joints are active (hip and ankle) and two joints are passive (knee and biarticular mechanism). Segments 1, 2 and 3 are arranged in a pantograph configuration. Segment 1 is driven by the hip motor, which is the main actuation of the robot. The hip motor, equipped

TABLE II
ROBOT DESIGN PARAMETERS.

Parameters		Value
Robot mass (config. A)*	m_A	1.05 kg
Robot mass (config. B)	m_B	1.20 kg
Leg resting length	l_0	408 mm
Segment 1 length	l_1	150 mm
Segment 2 length	l_2	150 mm
Segment 3 length	l_3	140 mm
Segment 4 length	l_4	70 mm
Knee pulley radius	r_k	30 mm
Knee spring stiffness	k_k	10.9 N/mm
Bi-articular insertion radius	r_{pk}	32 mm
Bi-articular spring stiffness	k_b	9.8 N/mm
Ankle pulley radius	r_a	15 mm
Ankle stiffness (air spring)	k_a	0.2 Nm/rad
Knee resting angle	α_0	130°
Ankle resting angle	β_0	175°
Hip swing amplitude	A	18°
Hip oscillation frequency	f	1.65 Hz

*the ankle motor is not removed from the robot torso.

with a 5:1 gearbox, swings the leg forward and backwards during locomotion. Segments 2 and 3 are passive, instead. The knee joint is passively extended to a resting angle of $\alpha_0 = 130^\circ$ by the knee spring k_k acting on the knee cam. Segment 3 is passively constrained by the spring-loaded biarticular segment k_b that acts over two joints, parallel to the shank, which replicates the lower leg muscle-tendon apparatus of gastrocnemius muscle and Achilles tendon. The overall under-actuated pantograph-like leg can be modeled as a non-linear spring that stores elastic energy during deceleration following the touch-down and converts spring energy back to kinetic energy which accelerates the robot in the second half of the stance phase. The proposed design parameters, which are summarized in Tab. II, are selected to meet the requirement of $\approx 10\%$ leg compression at three times body weight loading, similar to running dogs [34].

The design introduces our novel SELDA system to remotely actuate the foot (segment 4) for enhanced control of the interaction with the ground. SELDA exploits a second source of actuation, which is the proximally-mounted ankle motor. The motor torque is delivered to the ankle utilizing a lightweight pneumatic transmission, which also provides series elastic compliance and thus additional energy storage capabilities to the robot. Details of the working principle and the design of the SELDA system are provided in the following sections.

B. SELDA working principle

Starting from the concept of hydrostatic transmissions developed for the remote actuation of high-performance robots [35], we introduce a pneumatic rolling-diaphragm transmission (called SELDA) for the actuation of distal joints of a compliant robotic leg. The use of air instead of liquids, employed in other applications [27], makes it possible to merge functionalities of remote and series-elastic actuation in a single lightweight, efficient and compact device, showing convenient attributes such as low static friction, zero backlash, reduced complexity, and low-cost. A detailed scheme of the system is shown in Fig. 3 (left

and center). To minimize weight, we take advantage of the asymmetrical torque requirements of locomotion at the ankle joint, which provides large torques during the push-off phase and small torques for backward flexion during the swing phase. According to this consideration, the SELDA system is conceived as a single-acting device, able to transmit torques to the foot in the direction of the push-off. The flexion of the foot is passively actuated during the touch-down phase, when landing on the ground, as a result of the robot's weight/inertia. This allows the use of a single pneumatic cylinder placed distally, where mass reduction is critical, and one single cylinder placed in the proximal actuation group. Identical cylinders and pulleys (with radius r_a) are chosen at proximal and distal sides to determine a 1:1 static torque reflection between the remote motor and the ankle joint. The proposed cylinder units (i.e. cylinder, piston, rolling diaphragm and supporting frame) weight 42 g each, adding relatively low inertia distally.

The system is initially pressurized up to a bias pressure p_0 that acts on both cylinders in the direction of expansion (notice that diaphragms require the internal pressure to be always higher than the atmospheric pressure in any working condition to prevent the membrane jamming [25]). Torque T_a , generated by the motor, causes the proximal cylinder to compress and the air pressure p to increase. The pressure propagates through the pneumatic line up to the distal cylinder along the direction of expansion, generating a torque

$$T_A = r_a A_e p = T_0 + r_a A_e \Delta p \quad (1)$$

where constant A_e is the equivalent area of the diaphragm, $T_0 = r_a A_e p_0$ is the preload torque generated by the initial pressurization and Δp is the pressure increment due to volume variation $\Delta V = A_e r_a (\theta_A - \theta_a)$ generated by motor and ankle rotations. Experimental evidence in Sec. II-E shows that the assumption of adiabatic process well describes the response of SELDA, thus

$$T_A = r_a A_e p_0 V_0^\gamma / (V_0 + \Delta V)^\gamma, \quad (2)$$

where $\gamma = 1.4$ is the adiabatic index of air. A simpler description of the system is offered by the following linearised equation in the case of sufficiently small volume variations for the initial volume V_0 :

$$T_A \approx r_a A_e p_0 + \gamma r_a^2 A_e^2 \frac{p_0}{V_0} (\theta_a - \theta_A) = T_0 + k_a (\theta_a - \theta_A) \quad (3)$$

Indeed, the pneumatic transmission can be modeled as a linear spring with $k_a = \gamma r_a^2 A_e^2 p_0 / V_0$ stiffness and T_0 preload torque. Notice that (3) provides the lower bound of k_a , since the nonlinear response of air makes linearised stiffness larger for higher compression. In general, the system can be approximately modelled as a typical series-elastic system with 2-dof (Fig. 3 center), namely θ_a and θ_A . I_a and I_A are the inertia of proximal and distal bodies, which are connected by a torsional spring with stiffness k_a . It is worth noticing that this model offers a conservative estimation of the torque bandwidth of the actuation system, which is limited by the natural frequency $\omega_n = \sqrt{k_a / I_A}$.

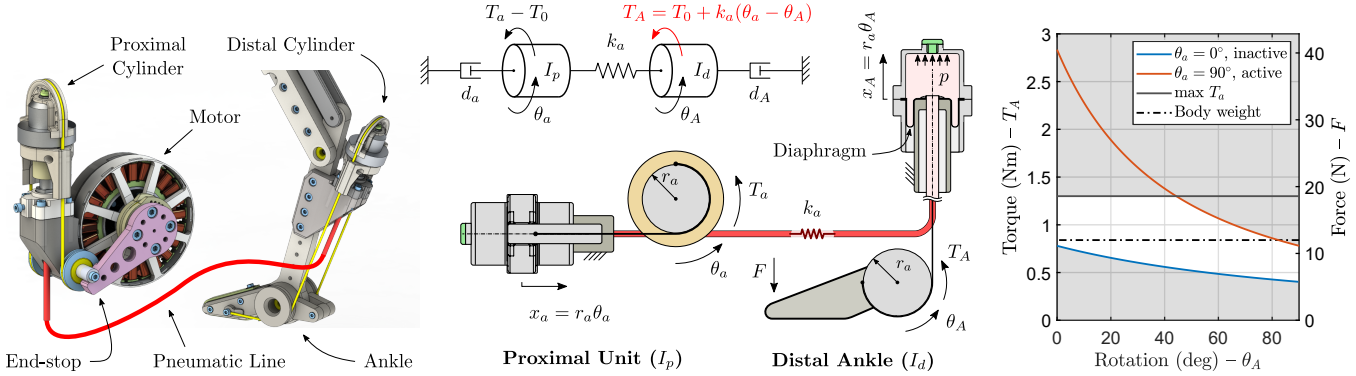


Fig. 3. SELDA system. *Left:* details of the proximal and distal units. *Center:* scheme and linearized description of the transmission system. *Right:* representation of the feasible range (in white background) of ankle torque T_A and foot force F as function of motor and ankle position.

C. SELDA dimensioning and details of implementation

Starting from kinematics observations, then confirmed by experiments in Fig. 6, we firstly impose a requirement on the minimum ankle rotation range of $\theta_A^m = 90^\circ$. With this choice, the use of rolling diaphragms poses an intrinsic design trade-off between added distal mass and transmission stiffness. Equation (3) suggests that the selection of membranes with large effective area A_e and thus longer stroke x_A^m (which allows for larger values of r_a) would produce higher stiffness and bandwidth. However, large-diameter cylinders come with larger distal mass, which degrades the locomotion dynamical properties. According to the relation between the diaphragm stroke, the required ankle rotation angle and the pulley radius, which reads as $\theta_A^m = x_A^m/r_a$, the choice of a small pulley radius r_a allows the use of smaller diaphragms (which have a limited stroke), leading to a lighter distal cylinder. However, the transmission stiffness (as well as the transmissible torque, for a given maximum motor torque) decreases. In this regard, an under-dimensioned low-stiffness air tendon is pursued, i.e., the torque T_A , which is transmitted to the foot, is not supposed to fully sustain the peak ground reaction force during stance (three times body weight, 36 N in our case). Thus, the presented design lets the inertial forces be absorbed by the heel, which touches the ground during stance like in many natural runners. Specifically, we set as a target the generation of a foot force F that is about able to balance the body weight in static conditions; ≈ 12 N. Because ground reaction forces drop to zero between mid-stance and lift-off, even small ankle torques from the active ankle actuation are expected to effectively alter the timing of the energy transfer to the ground during push-off and influence the hopping dynamics in terms of forward speed and hopping height. To meet these requirements, we select DM3-20-20 rolling diaphragms by Fujikura Composites (268.8 mm² effective area, 24 mm full stroke, 20 mm cylinder diameter). A pulley radius $r_a = 15$ mm guarantees a rotation range larger than 90°. A stiffness $k_a = 0.12$ Nm/rad and a torque bandwidth larger than 6 Hz (considered enough for open loop hopping) are obtained by selecting an initial pressure $p_0 = 0.1$ MPa. In the

passive configuration, i.e., the inactive SELDA-motor at the end-stop ($\theta_a = 0^\circ$), the force on the foot tip varies from $F = 6$ N when extended ($\theta_A = 90^\circ$), to $F = 11$ N when fully flexed ($\theta_A = 0^\circ$). This is also the force profile that is delivered when the foot lands on the ground. In the active configuration, when the SELDA motor fully compresses the proximal cylinder, the foot should generate a force of $F = 11$ N when extended and a force of $F = 42$ N when flexed. However, both are limited to 19 N by the maximum available motor torque. The workspace of feasible forces is highlighted in Fig. 3 (right), where achievable distal torques/forces are represented at different values of θ_a as a function of θ_A .

Hip and ankle joints are actuated by brushless motors (model MN7005-KV115) by *T-Motor* with 1.3 Nm maximum rated torque. The hip motor is equipped with an RS3505S planetary gearbox by *Matek* with 5:1 gear ratio. The motor positions are measured by AEAT8800-Q24 rotary encoders by *Broadcom* with 12 bit resolution. We use open-source drivers (Micro-Driver, [36]) for motor control, current sensing, and encoder reading. The Micro-Driver board is capable of dual motor Field Oriented Control (FOC) at 10 kHz. We implemented our controller on a single board computer (Raspberry Pi 3B+) with a control frequency of 1 kHz. The pneumatic line is implemented with a 70 mm long polyurethane hose with a $\phi 1.5$ mm inner diameter. The internal air volume of the transmission in the non-deformed configuration is 16.2 cm³. The knee and biarticular springs are implemented with SWS14.5-45 and UBB10-60 springs, respectively (*MISUMI*).

D. Experimental configurations

To investigate the influence of ankle actuation, i.e., power injection at distal joints on locomotion performances, two different leg configurations have been designed for testing and comparison (Fig. 1). 1) a configuration-A leg without actuated ankle and related components, which is equipped with a rubber foot directly connected to the segment 3; 2) a configuration-B leg which is fully equipped with the SELDA ankle actuation system described previously. The

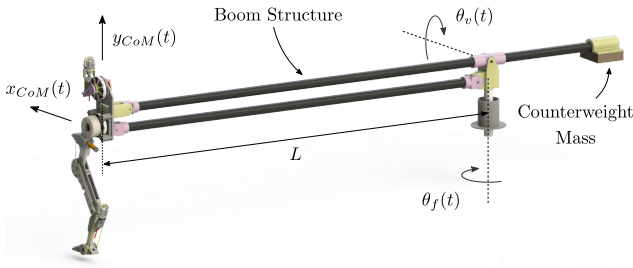


Fig. 4. Experimental test bench: the leg is constrained to a rotating boom to allow horizontal and vertical displacement only. Torso rotation and lateral displacement are prevented. The boom setup allows the robot to hop continuously over long distances.

configuration-A leg weighs less, i.e., in total 1.05 kg, due to the lack of the distal cylinder-ankle unit.

A custom setup that allows comparing both leg configurations and their locomotion patterns fairly was used for testing. The robot legs are minimally instrumented—torque and position measurements of distal joints are not used for control—and each actuator is controlled with feedforward reference trajectories, since locomotion stability and robustness are supported by compliant leg mechanics. Please see Sec. III for details. Initially, experiments of configuration-A are compared to those of the passive configuration-B. Configuration-B implements the SELDA system but its proximal ankle motor is inactive, to analyse the elastic foot contribution. Then, configuration-B is tested in the active mode to investigate the different activation timings of the ankle motor during the step cycle.

The trunk of the robot is mounted to a boom structure, Fig. 4 that prevents torso rotations, eliminating the need for trunk pitch control. The boom arm rotates around a vertical axis by angle θ_f , which allows the robot to jump along a circular path. The length of boom rods L is 1.55 m and the travelled distance over a complete revolution is 9.73 m. A counterweight balances the mass of boom rods. The position of the robot center of mass, x_{CoM} and y_{CoM} , are evaluated as a function of θ_f and θ_v angles. The boom rotation angles θ_f and θ_v are measured by two 102-V rotary encoders by AMT with 11 bit resolution.

E. Transmission characterization

To verify the SELDA model introduced in (2), we measured the motor torque while the foot segment was fixed at $\theta_A = 90^\circ$ and the actuator was progressively rotated along its full stroke. We manually applied a full-stroke rotation to the actuator rotor with an instrumented lever arm. A load cell (model 3133_0, Phidgets) was mounted to measuring the applied torque. Fig. 5 shows the measured data compared to model data (2), at a pre-pressurization of 0.1 MPa. Globally, the analytical model (2) well describes the behaviour of the experimental data, with observable mismatches due to hysteresis (Fig. 5). In separated experiments, we measured a motor friction/hysteresis of approximately 15 mNm to 25 mNm and a transmission friction/hysteresis due to diaphragms, cables and bearings of approximately

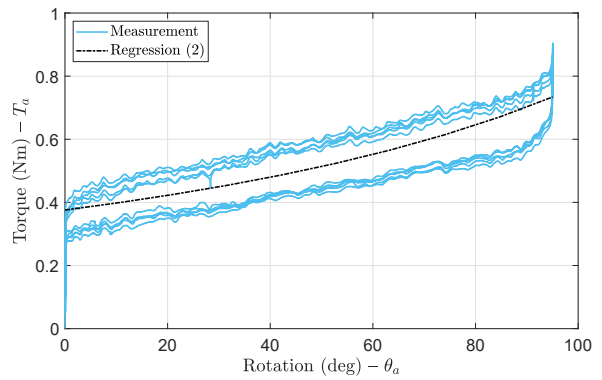


Fig. 5. Characterization of the input-actuation response of the SELDA system. The experimental data and the analytical model (2) are compared.

35 mNm to 50 mNm, explaining the observed hysteresis loop.

III. HOPPING EXPERIMENTS

This section presents our hopping experiments. Sec. III-A describes the experimental configuration chosen for gait analysis; Sec. III-B compares the performance of the leg with and without the foot segment, i.e., configuration-A and passive configuration-B; Sec. III-C presents our first investigation of the effect of distal actuation, mainly focusing on kinematic effects in terms of gait velocity, step length and step height. A typical gait obtained during the experiments with SELDA system is shown in Fig. 6.

A. Experimental configuration

The robot response is characterized in case of simple control strategies in order to emphasize intrinsic self-stabilizing response through compliant design. The hip joint is position controlled along a sinusoidal trajectory:

$$\hat{\theta}_H = A \sin(2\pi f t) \quad (4)$$

where constant A is the hip trajectory amplitude and constant f defines the hopping frequency. Hip oscillation amplitude $A = 18^\circ$ and locomotion frequency $f = 1.65$ Hz are common for all of our experiments. Note that the chosen parameter set is likely not optimal for both configurations; we expect that each configuration has its dynamics. Nevertheless, we keep the parameter common for a consistent comparison between leg configurations. An example hip trajectory is shown in Fig. 7. The trajectory tracking is performed through a PD controller $T_H = k_p e(t) + k_d \dot{e}(t)$, where T_H is the commanded torque to the hip joint and variable $e(t)$ is the tracking error $e(t) = \hat{\theta}_H - \theta_H$. The controller behaves like a virtual spring-damper element acting between the reference trajectory $\hat{\theta}_H$ and the hip joint with stiffness value k_p and damping coefficient k_d . Parameters $k_p = 40$ and $k_d = 0.35$ are fixed for all experiments.

To investigate the influence of the distal actuation, we focus on the actuation timing of the foot segment during the step cycle. A step torque reference of 1 Nm is commanded to the ankle motor: the initial actuation instant varies in the range 5 % to 30 % of the step cycle, as shown by the

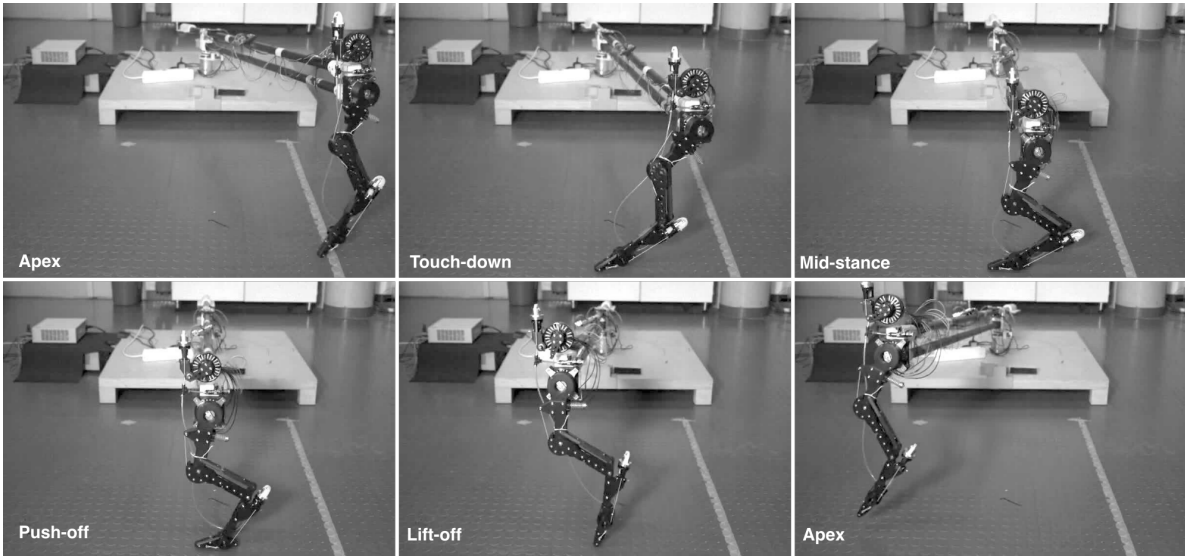


Fig. 6. Gait cycle snapshots from apex to apex, taken from high-speed video footage. A *delay* was programmed to trigger push-off actuation. Step cycle time ($T = 1/f$, f is frequency) is 606 ms, or 1.65 Hz hopping frequency.

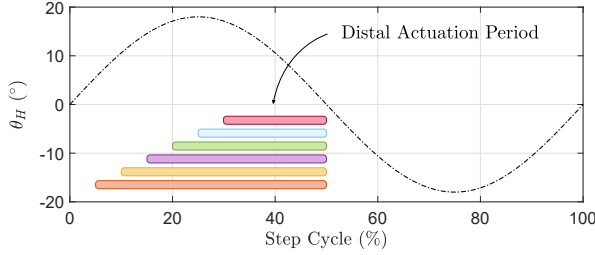


Fig. 7. Distal actuation timing with respect to the hip reference trajectory (black dashed line). The colored rectangles indicate the distal actuation period. Varying initial timing t_T values are considered: $t_T = 5\%, 10\%, 15\%, 20\%, 25\%$ and 30% of the step cycle. Distal actuation stops at 50 % of the step cycle, during the swing phase. Positive angles indicate a leg position behind the vertical axis (Fig. 2).

colored bars in Fig. 7; the ankle actuation is then ended at 50 % of the step cycle, during the swing phase when the leg is not in contact with the ground. The compliance features of the pneumatic transmission allow driving a simple step torque-reference to the ankle motor so that we can focus on analyzing the influence of actuation timing only.

B. Analysis of passive foot

In this section, leg configuration-B is tested in passive mode, i.e., without activating the ankle motor, and its performance is compared to configuration-A to assess the benefits of the additional compliant foot. Fig. 8 shows this comparison evaluated on data sets corresponding to a complete revolution of the circular trajectory around the boom. The top plot shows that the distance of 9.7 m is traveled in 15.7 s by robot configuration-A and in 8.1 s by the configuration-B in SELDA passive mode. In this experiment, SELDA increases the forward velocity \dot{x}_{CoM} from 0.62 m/s to 1.20 m/s; an almost two-fold increase. The higher-speed locomotion is also visible in terms of step length, Fig. 8 (bottom-left), which increases of 93 % from 378 mm to 730 mm. The foot

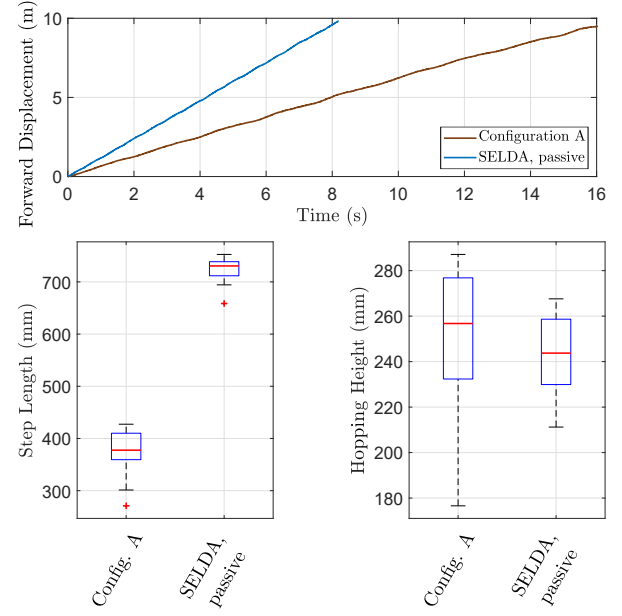


Fig. 8. Performance comparison between configurations-A and -B, (Fig. 1). In this experiment the distal segment is not actuated and the pneumatic transmission behaves like an air spring. *Top*: time to travel a complete turn around the boom. *Left*: statistical analysis of the maximum step height over one full boom revolution. *Right*: statistical analysis of the step length over one full revolution.

slightly affects the robot's maximum hopping height (Fig. 8 bottom-right), but it leads to a more repeatable hopping height and more stable hopping motion. Based on the ankle's stiffness characterization of Fig. 5, we estimate 67 mJ of peak energy stored in the ankle joint. In comparison, we calculate the hip's virtual spring peak energy of 250 mJ.

C. Analysis of active foot

This section investigates the effect of the SELDA activation timing, also in comparison with the passive foot

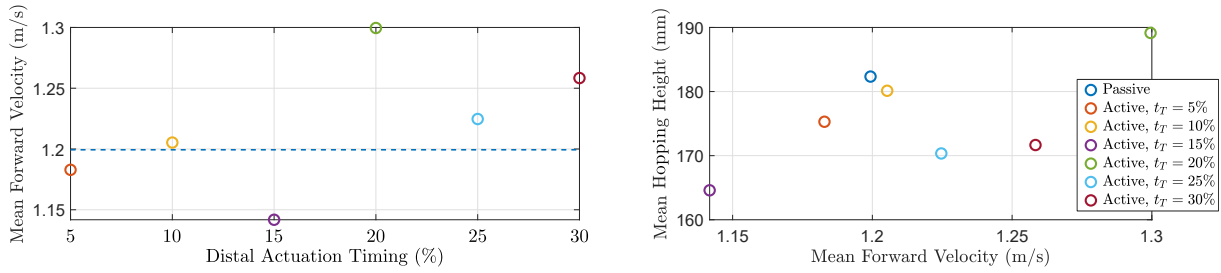


Fig. 9. Investigation of the effect of different distal actuation timing t_T . *Left:* mean velocity of the center of mass achieved for different values of timing t_T . The blue dashed line refers to measurements obtained with the passive-mode system. *Right:* mean step height with respect to mean forward velocity. Step height is the difference between the highest and the lowest vertical position of the robot's center of mass at each step. Mean values refer to the dataset corresponding to one full revolution around the boom (9.7 m travelled distance) during steady state locomotion.

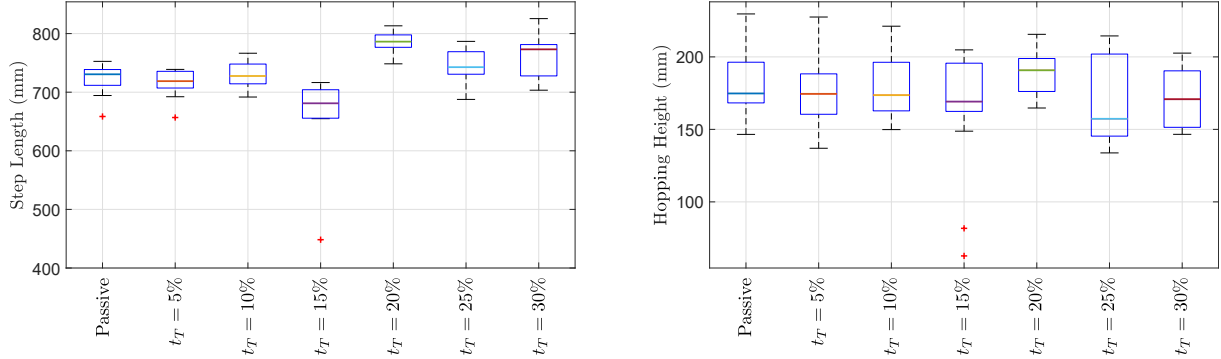


Fig. 10. Box plot statistical representation of the influence of distal actuation timing t_T on step length and maximum step height. The dataset of this analysis corresponds to samples collected during one full revolution around the boom in steady state gait. The minimum number of steps for one revolution is 13.

configuration. The initial timing t_T of the ankle actuation varies in the range 5 % to 30 % of the step cycle; a timing of 5 % means that the ankle is actuated right after the touchdown, while the timing of 30 % means that the ankle is actuated right before the lift-off. Fig. 9 (left) shows that, in general, the center-of-mass velocity \dot{x}_{CoM} can be increased by activating the ankle after mid-stance, while it is slowed down by actuating the ankle before mid-stance. In particular, the active SELDA achieves the highest forward velocity of 1.30 m/s with an actuation timing of $t_T = 20\%$ versus a speed of $\dot{x}_{CoM} = 1.20$ m/s for the passive SELDA. The lowest performance is observed with an actuation timing of $t_T = 15\%$ leading to an average forward speed of $\dot{x}_{CoM} = 1.14$ m/s. Fig. 9 (right) illustrates the energy transfer between hopping height and forward velocity \dot{x}_{CoM} . The hopping height is calculated at each step as the difference between the highest and the lowest vertical position y_{CoM} reached by the robot's center of mass. By tuning the activation timing, we can effectively adjust the hopping height by 11 % and the forward velocity by 14 %. Note that our diaphragm actuation produces a torque of (≈ 1 Nm) from the motor side, which also compensates for the internal pressure of the pneumatic line. Albeit the limited actuator output torque, we observe that locomotion speed and hopping height are effectively altered (Fig. 9 left and right). We quantify the effect of the activation timing in terms of step length and hopping height over a minimum number of 13 steps, i.e. one revolution, during steady state locomotion

(Fig. 10). Narrow bands in the box plot indicate a more stable hopping gait. We observed period-2 hopping in some experiments, which expands the confidence interval in the plot. Once gait parameters such as frequency and amplitude are tuned to match the robot's dynamic, we expect to further reduce the variation of step length and hopping height.

The supplementary video of the robot leg with SELDA actuated ankle joint can also be found at this YouTube link.

IV. CONCLUSIONS

This work proposes distal actuation of the foot segment in a bio-inspired hopping robot with a compliant rolling diaphragm pneumatic transmission. Diaphragm actuation has appealing features of lightweight, low-friction, high efficiency, and truly remote actuation. We found self-stabilizing gaits with comparatively simple, open-loop position control. We show that the addition of a foot segment improves the locomotion performance of the robot, already in its passive elastic mode, with an increase in forward velocity of 93 %. With the actuated foot, we observed that actuation timing effectively influences the hopping gait. By tuning the ankle actuation timing from 5 % to 30 % of the gait cycle, we observed a 11 % change in hopping height and 14 % change in forward velocity, with its currently under-dimensioned actuator. Based on these first results, our future developments will focus on providing the proximal cylinder with an antagonistic action to reduce the actuation effort that is required to balance the hose's internal pressure. An

additional gearbox mounted to the ankle motor will increase output torque at reduced electrical power requirements. The proposed experiments are not yet based on optimal control strategies, and we expect SELDA to achieve higher performance in the future. Gait patterns will be optimized for energy efficient and agile locomotion, by tuning control parameters and type, and by introducing online feedback.

REFERENCES

- [1] R. M. Alexander, "Elastic Energy Stores in Running Vertebrates," *American Zoologist*, vol. 24, no. 1, pp. 85–94, Jan. 1984.
- [2] R. Alexander, "Three Uses for Springs in Legged Locomotion," *The International Journal of Robotics Research*, vol. 9, no. 2, pp. 53–61, Apr. 1990.
- [3] H. Witte, H. Hoffmann, R. Hackert, C. Schilling, M. S. Fischer, and H. Preuschoft, "Biomimetic robotics should be based on functional morphology," *Journal of Anatomy*, vol. 204, no. 5, pp. 331–342, May 2004.
- [4] J. Pratt and G. Pratt, "Intuitive control of a planar bipedal walking robot," in *1998 IEEE International Conference on Robotics and Automation, 1998. Proceedings*, vol. 3, 1998, pp. 2014–2021 vol.3.
- [5] M. S. Fischer, N. Schilling, M. Schmidt, D. Haarhaus, and H. Witte, "Basic limb kinematics of small therian mammals," *J Exp Biol*, vol. 205, no. 9, pp. 1315–1338, May 2002.
- [6] A. J. Ijspeert, "Central pattern generators for locomotion control in animals and robots: A review," *Neural Networks*, vol. 21, no. 4, pp. 642–653, May 2008.
- [7] A. Badri-Spröwitz, A. Aghamaleki Sarvestani, M. Sitti, and M. A. Daley, "Birdbot achieves energy-efficient gait with minimal control using avian-inspired leg clutching," *Science Robotics*, vol. 7, no. 64, p. eabg4055, 2022.
- [8] B. Kiss, E. C. Gonen, A. Mo, A. Buchmann, D. Renjewski, and A. Badri-Spröwitz, "Gastrocnemius and power amplifier soleus spring-tendons achieve fast human-like walking in a bipedal robot," no. arXiv:2203.01588, Mar. 2022.
- [9] Y. P. Ivanenko, R. E. Poppele, and F. Lacquaniti, "Five basic muscle activation patterns account for muscle activity during human locomotion," *The Journal of Physiology*, vol. 556, no. 1, pp. 267–282, 2004.
- [10] F. De Groote, I. Jonkers, and J. Duysens, "Task constraints and minimization of muscle effort result in a small number of muscle synergies during gait," *Frontiers in Computational Neuroscience*, vol. 8, p. 115, 2014.
- [11] J. M. Caputo and S. H. Collins, "Prosthetic ankle push-off work reduces metabolic rate but not collision work in non-amputee walking," *Scientific Reports*, vol. 4, no. 1, May 2015.
- [12] G. S. Sawicki and D. P. Ferris, "A pneumatically powered knee-ankle-foot orthosis (KAFO) with myoelectric activation and inhibition," *Journal of NeuroEngineering and Rehabilitation*, vol. 6, no. 1, p. 23, Jun. 2009.
- [13] O. B. Farah, Z. Guo, C. Gong, C. Zhu, and H. Yu, "Power analysis of a series elastic actuator for ankle joint gait rehabilitation," in *2015 IEEE International Conference on Robotics and Automation (ICRA)*, May 2015, pp. 2754–2760.
- [14] M. Ishikawa, P. V. Komi, M. J. Grey, V. Lepola, and G.-P. Brugemann, "Muscle-tendon interaction and elastic energy usage in human walking," *Journal of Applied Physiology*, vol. 99, no. 2, pp. 603–608, Aug. 2005.
- [15] S. W. Lipfert, M. Günther, D. Renjewski, and A. Seyfarth, "Impulsive ankle push-off powers leg swing in human walking," *The Journal of experimental biology*, vol. 217, no. 8, pp. 1218–1228, 2014.
- [16] P. Cherelle, V. Grosu, M. Cestari, B. Vanderborght, and D. Lefeber, "The AMP-Foot 3, new generation propulsive prosthetic feet with explosive motion characteristics: design and validation," *BioMedical Engineering OnLine*, vol. 15, p. 285, 2016.
- [17] H. Mineshita, T. Otani, K. Hashimoto, M. Sakaguchi, Y. Kawakami, H. O. Lim, and A. Takanishi, "Robotic Ankle Mechanism Capable of Kicking While Jumping and Running and Adaptable to Change in Running Speed," in *2019 IEEE-RAS 19th International Conference on Humanoid Robots (Humanoids)*, Oct. 2019, pp. 505–510.
- [18] M. Hutter, C. D. Remy, M. A. Hoepflinger, and R. Siegwart, "Efficient and versatile locomotion with highly compliant legs," *IEEE/ASME Transactions on Mechatronics*, vol. 18, no. 2, pp. 449–458, 2012.
- [19] B. Katz, J. Di Carlo, and S. Kim, "Mini cheetah: A platform for pushing the limits of dynamic quadruped control," in *2019 International Conference on Robotics and Automation (ICRA)*. IEEE, 2019, pp. 6295–6301.
- [20] S. Rutishauser, A. Spröwitz, L. Righetti, and A. Ijspeert, "Passive compliant quadruped robot using central pattern generators for locomotion control," in *Proceedings of 2nd IEEE RAS & EMBS International Conference on Biomedical Robotics and Biomechatronics (Biorob)*. Scottsdale, AZ, USA: IEEE Biorob 2008, Oct. 2008.
- [21] M. H. Raibert, "Trotting, pacing and bounding by a quadruped robot," *Journal of Biomechanics*, vol. 23, no. Supplement 1, pp. 79–81, 1990.
- [22] C. Semini, N. G. Tsagarakis, E. Guglielmino, M. Focchi, F. Cannella, and D. G. Caldwell, "Design of HyQ-a hydraulically and electrically actuated quadruped robot," *Proceedings of the Institution of Mechanical Engineers, Part I: Journal of Systems and Control Engineering*, vol. 225, no. 6, pp. 831–849, 2011.
- [23] K. Narioka, A. Rosendo, A. Spröwitz, and K. Hosoda, "Development of a Minimalistic Pneumatic Quadruped Robot for Fast Locomotion," in *Proceedings of IEEE International Conference on Robotics and Biomimetics (ROBIO)*, Guangzhou, China, 2012, pp. 307–311.
- [24] R. Niyyama, A. Nagakubo, and Y. Kuniyoshi, "Mowgli: A Bipedal Jumping and Landing Robot with an Artificial Musculoskeletal System," in *2007 IEEE International Conference on Robotics and Automation*, 2007, pp. 2546–2551.
- [25] J. P. Whitney, M. F. Glisson, E. L. Brockmeyer, and J. K. Hodgins, "A low-friction passive fluid transmission and fluid-tendon soft actuator," in *Intelligent Robots and Systems (IROS 2014), 2014 IEEE/RSJ International Conference on*. IEEE, 2014, pp. 2801–2808.
- [26] J. Hepp and A. Badri-Spröwitz, "A Novel Spider-Inspired Rotary-Rolling Diaphragm Actuator with Linear Torque Characteristic and High Mechanical Efficiency," *Soft Robotics*, Jun. 2021.
- [27] M. Bolignari and M. Fontana, "Design and experimental characterization of a high performance hydrostatic transmission for robot actuation," *Meccanica*, vol. 55, no. 5, pp. 1169–1179, 2020.
- [28] S. Frishman, R. D. Ings, V. Sheth, B. L. Daniel, and M. R. Cutkosky, "Extending reach inside the mri bore: A 7-dof, low-friction, hydrostatic teleoperator," *IEEE Transactions on Medical Robotics and Bionics*, vol. 3, no. 3, pp. 701–713, 2021.
- [29] A. Mo, F. Izzi, D. F. B. Haeufle, and A. Badri-Spröwitz, "Effective Viscous Damping Enables Morphological Computation in Legged Locomotion," *Frontiers in Robotics and AI*, vol. 7, 2020.
- [30] J. P. Whitney, T. Chen, J. Mars, and J. K. Hodgins, "A hybrid hydrostatic transmission and human-safe haptic telepresence robot," in *Robotics and Automation (ICRA), 2016 IEEE International Conference on*. Stockholm, Sweden: IEEE, 2016, pp. 690–695.
- [31] C. Hubicki, J. Grimes, M. Jones, D. Renjewski, A. Spröwitz, A. Abate, and J. Hurst, "Atrias: Design and validation of a tether-free 3d-capable spring-mass bipedal robot," *The International Journal of Robotics Research*, vol. 35, no. 12, pp. 1497–1521, 2016.
- [32] F. Ruppert and A. Badri-Spröwitz, "Series Elastic Behavior of Biarticular Muscle-Tendon Structure in a Robotic Leg," *Frontiers in Neurorobotics*, vol. 13, p. 64, Aug. 2019.
- [33] A. Spröwitz, A. Tuleu, M. Vespiagnani, M. Ajallooeian, E. Badri, and A. Ijspeert, "Towards Dynamic Trot Gait Locomotion: Design, Control and Experiments with Cheetah-cub, a Compliant Quadruped Robot," *Int. J. of Robotics Research*, vol. 32, no. 8, pp. 932–950, 2013.
- [34] R. M. Walter and D. R. Carrier, "Ground forces applied by galloping dogs," *Journal of Experimental Biology*, vol. 210, no. 2, pp. 208–216, 2007.
- [35] M. Bolignari, G. Rizzello, L. Zaccarian, and M. Fontana, "Smith-predictor-based torque control of a rolling diaphragm hydrostatic transmission," *IEEE Robotics and Automation Letters*, vol. 6, no. 2, pp. 2970–2977, 2021.
- [36] F. Grimmerger, A. Meduri, M. Khadiv, J. Viereck, M. Wüthrich, M. Naveau, V. Berenz, S. Heim, F. Widmaier, T. Flayols, J. Fiene, A. Badri-Spröwitz, and L. Righetti, "An open torque-controlled modular robot architecture for legged locomotion research," *IEEE Robotics and Automation Letters*, vol. 5, no. 2, pp. 3650–3657, 2020.